Electron–Phonon Coupling in CdSe Nanocrystals from an Atomistic Phonon Model

Anne Myers Kelley*

School of Natural Sciences, University of California, Merced, 5200 North Lake Road, Merced, California 95343, United States

ABSTRACT Phonon frequencies and eigenvectors, electron–phonon couplings, and the associated resonance Raman spectra have been calculated for approximately spherical, wurtzite form CdSe nanocrystals having radii of 1.4 to 2.3 nm and containing 318 to 1498 atoms. Calculations of the equilibrium geometries and phonon modes are carried out using an empirical force field, and the electron and hole wave functions are calculated as particle-in-a-sphere envelope functions multiplying the Bloch functions, with valence-band mixing included for the hole functions. The coupling of each phonon mode to the $1S_e-1S_{3/2}$ and $1S_e-2S_{3/2}$ excitations is evaluated directly from the change in Coulombic energy along the phonon coordinate. Ten to 50 different modes in each crystal have significant Huang–Rhys factors, clustered around two frequency regions: acoustic phonons at 20–40 cm^{-1} depending on crystal size, and optical phonons at 185–200 cm^{-1}. The Huang–Rhys factors are larger for the acoustic modes than for the optical modes and decrease with increasing crystal size, and the Huang–Rhys factors for each group of modes are smaller for the $1S_e-2S_{3/2}$ than for the $1S_e-1S_{3/2}$ excitation. These results are compared with measurements of electron–phonon coupling in CdSe nanocrystals using different experimental techniques.

KEYWORDS: electron–phonon coupling · CdSe nanocrystal · resonance Raman · semiconductor nanoparticle · Huang–Rhys factor

Electron–phonon coupling (EPC) refers to the dependence of electronic-state energies on displacement of the nuclei along a phonon coordinate. Distorting the nuclei changes the energy gaps between electronic states and therefore modulates electronic relaxation processes. Electronic excitation also induces nuclear motion by changing the equilibrium nuclear positions from their ground-state values. The magnitude of EPC is typically expressed through the Huang–Rhys factor S, which is the ratio of one-phonon to zero-phonon intensity in the low-temperature optical spectrum. $S = \Delta^2/2$, where Δ is the displacement between the ground- and excited-state potential minima along the dimensionless phonon coordinate q, where $q = 1$ at the classical turning point in the vibrational ground state (*i.e.*, when the dimensionless phonon coordinate is unity, the vibrational potential energy equals the total vibrational zero-point energy).

The magnitude and frequency distribution of electron–phonon coupling contributes to the time scales and efficiencies of several photophysical processes of fundamental and technological significance in semiconductor nanocrystals (SC NCs). These include carrier multiplication, the process whereby absorption of one high-energy photon produces two or more electron–hole pairs instead of dissipating the excess photon energy as heat;[1−4] interfacial charge separation, the transfer of an electron or hole from a SC NC to a molecular acceptor on the surface[5] or across a heterojunction between two different semiconductors;[6−8] and other processes that depend on the time scales for dissipation of the excess energy of charge carriers. Accordingly, the magnitude of EPC in SC NCs and its dependence on NC composition, size, and shape are interesting and relevant questions. Phonons in SC NCs are usually treated as being similar to those of the bulk materials, the most important difference arising from the reduced translational symmetry of the NC. The phonons no longer have well-defined wave vectors, leading to changes in selection rules, and NCs have surface modes not present in the bulk. Electronic excitations in SC NCs also differ from those in the bulk material as evidenced by, for example, the energy shifts caused by quantum confinement. Thus the magnitudes and phonon frequency distributions of EPC in NCs may differ from those in the bulk for reasons related to differences in both the phonons and the charge carrier excitations. Yet despite many experimental and theoretical studies of EPC in SC NCs, little consensus has emerged from them.[9] This paper deals exclusively with coupling of phonons to electron–hole pairs (excitons), not to intraband transitions of isolated electrons[10] or holes.

This work focuses on the widely studied II–VI semiconductor, cadmium selenide.

* Address correspondence to amkelley@ucmerced.edu.

Received for review April 21, 2011 and accepted May 17, 2011.

Published online May 17, 2011
10.1021/nn201475d

The phonons of CdSe NCs are assigned as longitudinal optical (LO) phonons near 210 cm^{-1},[11,24] transverse and surface optical modes at slightly lower frequencies,[11−14] and acoustic phonons at still lower frequencies.[20−25] The optical phonon frequencies are quite similar to those in bulk CdSe, while the acoustic frequencies depend strongly on particle size. Standard dielectric continuum models attribute EPC for optical phonons to the Fröhlich interaction, in which the phonons generate a macroscopic oscillating polarization that modulates the periodic potential that determines the electronic band energies.[11,26] Acoustic modes are coupled through the deformation potential (the shift in the electronic band energies caused by a static displacement of the atomic positions) and the piezoelectric potential (the macroscopic electric polarization induced by an acoustic vibration).[26−28] As discussed by Alivisatos *et al.*,[15] both calculation of the Fröhlich interaction and analysis of the resonance Raman overtone progression for the longitudinal optical (LO) phonon in bulk CdSe yield $S \sim 10$ (note that eq 3 of this reference implies the definition $S = \Delta^2$, not $\Delta^2/2$). In strongly confined NCs, where the electron and hole wave functions have greater spatial overlap, most calculations predict $S < 0.1$ for both acoustic and optical phonons.[27,29,30] The coupling has variously been predicted to be independent of NC size,[11] to increase with decreasing size,[26,28] or to have a more complicated size dependence.[27,29,31] Experimentally, EPC for electron−hole pairs has been studied in II−VI semiconductor NCs through several techniques as summarized in ref 9. The experimental S values reported for the LO phonon of spherical CdSe NCs range from <0.02 to 0.5, considerably smaller than for bulk CdSe,[15] but the range of values obtained for both the optical and acoustic phonons of particles of similar size is more than an order of magnitude.[12,15,19−21,24,27,32,33] Some recent studies find the EPC to be stronger for optical than for acoustic phonons,[24] while others find the reverse.[20,21] Size-dependent studies have found S for the LO phonon to be essentially independent of NC size,[11,13] to increase with decreasing size,[17,33] and to decrease with decreasing size.[20] Different coupling strengths for different excitonic states may also be a confounding factor that has not been considered in most studies. The coupling to both acoustic and particularly optical phonons has been reported to be a strong function of excitonic state, becoming weaker for higher-lying states.[20,21]

Most discussions of SC NC phonons adopt a macroscopic picture which treats them as confined versions of the bulk crystal phonons. Atomistic simulations of phonon frequencies using empirical potentials have been reported for GaP,[34] Ge,[35] InAs,[36] SiGe,[37] and GaAs/AlAs core−shell NCs[38] with thousands of atoms. None of those studies addressed EPC, although an atomistic phonon model was coupled with a bond polarizability approach to calculate the size dependence of nonresonant Raman intensities in Si quantum dots,[39] and pseudopotential density functional calculations have been used to calculate nonresonant Raman spectra in Si NCs with several hundred atoms.[40] In this paper, a well-tested empirical force field for CdSe[41] is employed to calculate equilibrium geometries and phonon frequencies and eigenvectors for model CdSe nanocrystals having up to 1498 atoms (particle radius ∼2.3 nm). These phonon modes are combined with the electron and hole wave functions generated from an envelope function/Bloch function model for the electron and hole wave functions to compute the electron−phonon coupling strengths for each phonon mode. These EPCs are then used to calculate the resonance Raman spectra.

RESULTS AND DISCUSSION

Calculations were performed on 15 stoichiometric CdSe nanocrystals ranging in radius from 1.4 to 2.3 nm and consisting of 318 to 1498 atoms. Calculations were also performed on four nonstoichiometric NCs of about 2.3 nm radius having a net excess of up to 10 cations or up to 11 anions. Figure 1 shows the minimized structures of several representative stoichiometric crystals. All of the structures are roughly spherical and predominantly crystalline, but there is considerable surface reconstruction. For the purpose of calculating the electronic wave functions, the NCs were taken to be spherical with a radius equal to that of the most distant atom.

The calculated phonon frequencies range from near 0 to slightly under 300 cm^{-1}. The phonon density of states is very similar for all sizes of NCs examined, as shown in Figure 2. From about 30−220 cm^{-1}, there are no gaps or very sparse regions in the phonon density of states. Visual inspection of the normal modes reveals considerable variety in the nature of the motions, particularly with regard to the extent of delocalization of the modes. Modes with nearly degenerate frequencies are in some cases highly delocalized over the entire crystal and in other cases largely localized to just a handful of atoms. In this regard, the phonons of even the largest clusters have more in common with vibrations of large molecules than with confined versions of the phonons of a perfect bulk crystal.

Figure 3 plots the distribution of Huang−Rhys factors in both the $1S_e-1S_{3/2}$ and $1S_e-2S_{3/2}$ transitions for three representative structures spanning the size range examined. Most of the active modes can be divided into a group in the acoustic frequency range from 10 to 75 cm^{-1} and a group in the optical frequency range from 170 to 210 cm^{-1}. Modes at intermediate frequencies exhibit very weak EPC despite being well represented in the phonon density of states (Figure 2). All structures examined have a number of modes with significant EPC. Each NC has between

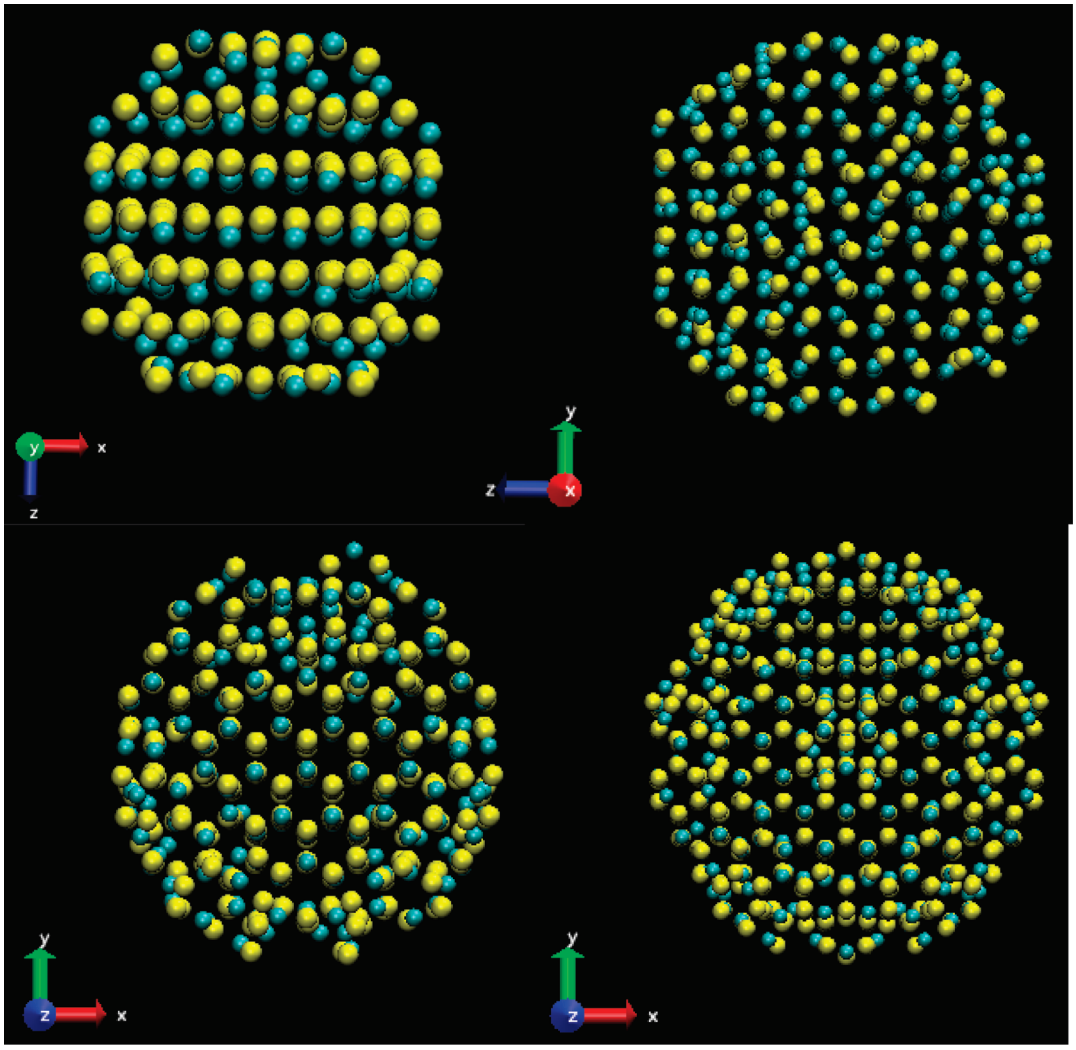

Figure 1. Top row: structures with 326 atoms (left) and 1204 atoms (right), viewed along the *y* and *x* axes, respectively. Bottom row: structures with 746 atoms (left) and 1482 atoms (right) viewed along the *z* axis. Blue atoms are Cd and yellow are Se.

10 and 50 different modes for which the Huang–Rhys factors *S* are within a factor of 10 of the largest single one. The actual number of different modes with significant *S* values is similar in large and small NCs, but the active modes span a narrower range of frequencies in the larger crystals. Direct comparison of these "EPC spectra" to experimental high-resolution electronic spectra of CdSe NCs is complicated by the band-edge exciton fine structure.[1,32,42] The $1S_e-1S_{3/2}$ transition, eight-fold degenerate in a simple model, is split by the crystal field and the electron–hole exchange interaction into five sublevels. Three of these are dipole-allowed, giving rise to additional fine structure in the high-resolution photoluminescence excitation spectra that complicates observation of the vibronic structure. The lowest of the five levels for nearly spherical NCs is a dipole-forbidden "dark exciton", and single-particle or line-narrowed emission at very low temperatures occurs through phonon-assisted mechanisms which produce a different vibronic intensity pattern from a simple Franck–Condon progression. For these reasons, we have not attempted to compare the results of these calculations to experimental spectra.

The maximum *S* for any single phonon mode ranges from 0.4 to 0.8 for the smallest NCs to 0.15–0.35 for the largest ones and varies considerably even among NCs of similar size. A more useful measure of EPC is the sum of the Huang–Rhys factors for all modes in a given frequency range, a quantity that is much more constant among different structures of similar size. (The fraction of the total absorption or emission intensity in the electronic origin is given by $\exp(-\sum S_i)$.) The phonons have been grouped into those with frequencies below 100 cm^{-1} and above 100 cm^{-1}, corresponding roughly to the acoustic and optical modes, respectively. The sum of the Huang–Rhys factors for the acoustic modes in the $1S_e-1S_{3/2}$ transition ranges from about 7 for the smallest NCs to about 2 for the largest ones, as shown in Figure 4. For the $1S_e-2S_{3/2}$ transition, the acoustic mode couplings are smaller but follow the same trend with NC size. For the optical modes in the $1S_e-1S_{3/2}$ transition, this sum ranges from about 1.2

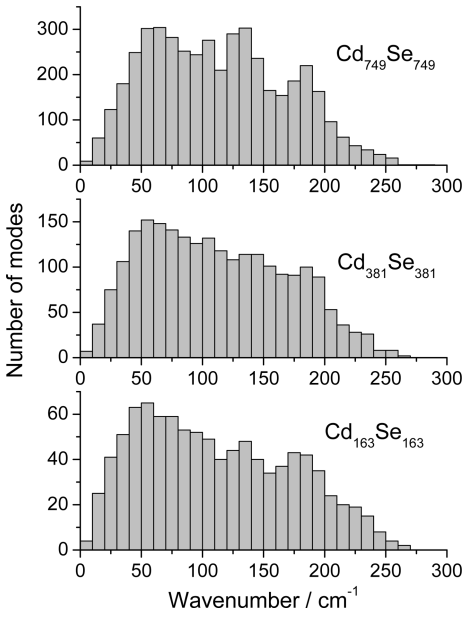

Figure 2. Phonon density of states for three representative NCs.

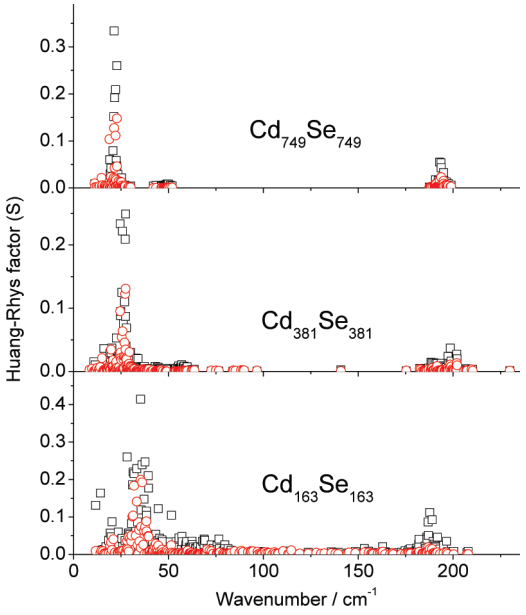

Figure 3. Distribution of Huang–Rhys factors for three representative NCs with the indicated stoichiometries and radii of 1.39, 1.88, and 2.28 nm. Black squares, $1S_e-1S_{3/2}$ transition; red circles, $1S_e-2S_{3/2}$ transition.

for the smallest NCs to about 0.55 for the largest ones (Figure 5). The average Huang–Rhys factor per mode varies even more strongly with size, dropping by an order of magnitude from the smallest to the largest NCs. The optical mode couplings are considerably smaller for the $1S_e-2S_{3/2}$ transition and have only a weak dependence on NC size. Results are not shown for the nonstoichiometric structures, but no significant systematic differences were observed in either the phonon frequencies or the coupling strengths between stoichiometric

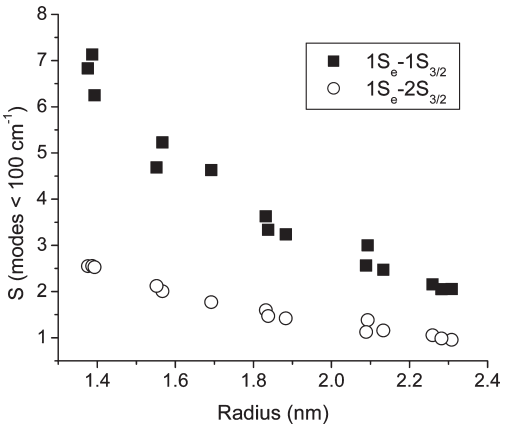

Figure 4. Sum of Huang–Rhys factors for all phonon modes below 100 cm^{-1} as a function of NC size for the two electron–hole states considered.

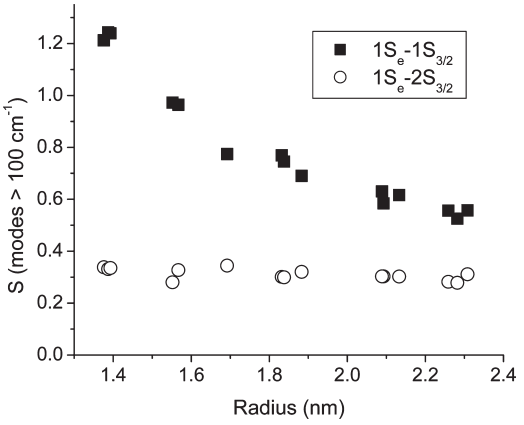

Figure 5. Same as Figure 2, for the modes above 100 cm^{-1}.

and nonstoichiometric structures in the 1400–1500 atom size range.

Figure 6 shows the resonance Raman spectra calculated for three different NCs spanning the same size range as those in Figure 3, assuming resonance with both the $1S_e-1S_{3/2}$ and $1S_e-2S_{3/2}$ excitations. The optical modes are comparatively much more prominent in the Raman spectra than in Figure 3 because the ω^2 weighting of the Raman intensities suppresses the relative intensities of the lower-frequency modes. The $1S_e-2S_{3/2}$ resonant spectra are qualitatively similar to the $1S_e-1S_{3/2}$ spectra. As shown in Figure 3, with increasing NC size, the coupled modes become more tightly clustered into a small range of frequencies, making the Raman spectra of the larger NCs appear simpler.

Figure 7 summarizes the frequencies of the low-frequency and high-frequency peaks in the calculated $1S_e-1S_{3/2}$ resonance Raman spectra for all 15 stoichiometric NCs examined. The lowest-frequency acoustic mode moves to lower frequencies as the NC size increases, as expected.[20,21,25,27,43,44] The effective frequency of the principal coupled optical modes, however, exhibits no clear trend with NC size.

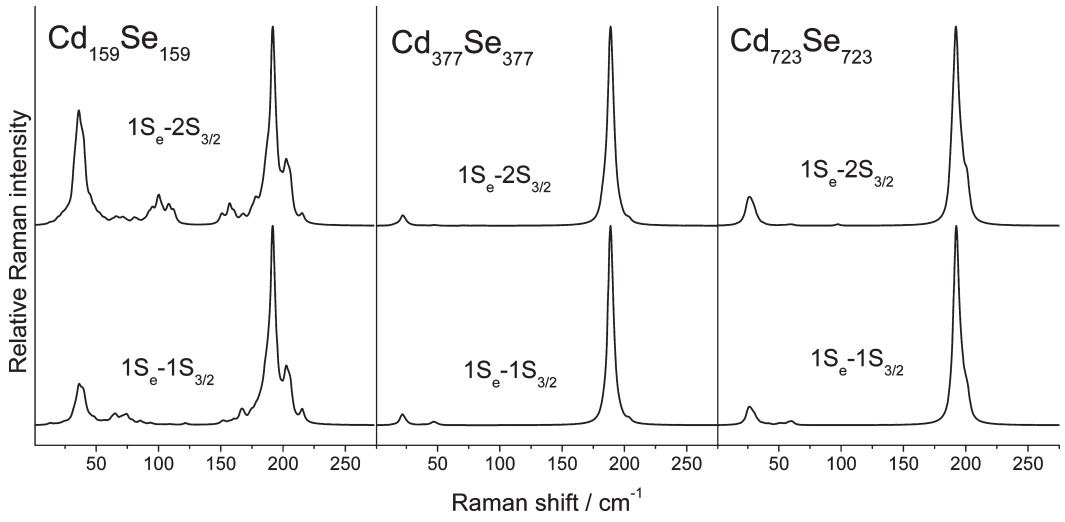

Figure 6. Calculated Raman spectra for three representative NCs with radii of 1.38, 1.84, and 2.26 nm, on resonance with the three indicated transitions.

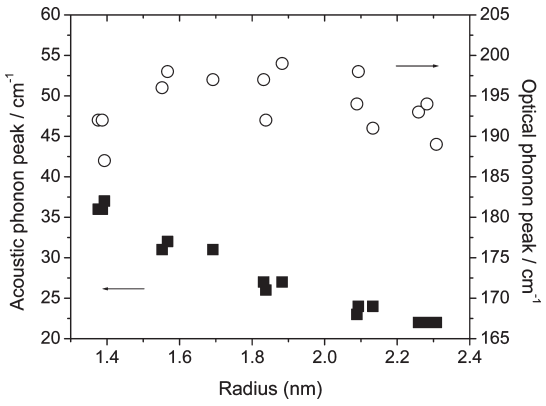

Figure 7. Frequencies of the lowest acoustic phonon peak (left-hand axis, squares) and the optical phonon peak (right-hand axis, circles) in the simulated $1S_e-1S_{3/2}$ resonance Raman spectrum as a function of NC radius.

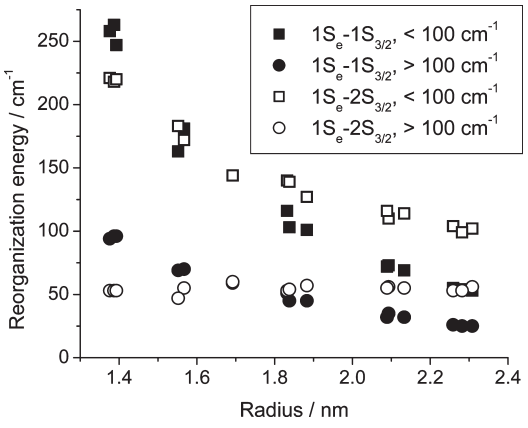

Figure 8. Sum of reorganization energies for all phonon modes below 100 cm^{-1} and above 100 cm^{-1} as a function of NC size for the two electron−hole states considered.

The Huang−Rhys factor, while perhaps the simplest measure of electron−phonon coupling, may not be the most relevant one. For many purposes, a better measure is the reorganization energy $\lambda = \hbar\omega S$,[45] the energy difference between the electronically excited configuration at the vertical (ground-state) geometry and at the relaxed excited-state geometry. The reorganization energy determines the phonon contribution to the optical transition bandwidth and to the rate constant for nonradiative processes. Figure 8 displays the total reorganization energy in low-frequency and high-frequency modes for both excitations. In both states, the acoustic and optical modes make fairly similar contributions to the reorganization energy, with the acoustic modes dominating at small NC sizes and the optical modes becoming more important for larger crystals. For comparison, the reorganization energy associated with the LO phonon in bulk CdSe, using the reported Huang−Rhys factor of $S \sim 10$,[15] is $\lambda \sim 2100\ cm^{-1}$.

The clearest conclusion from this work is that the overall electron−phonon coupling strength for these approximately spherical CdSe nanocrystals decreases monotonically with increasing size over the range of 1.4 to 2.3 nm radius. This conclusion holds for both acoustic and optical phonons for the lowest-energy $1S_e-1S_{3/2}$ electron−hole excitation and also holds at least for the acoustic phonons for $1S_e-2S_{3/2}$ excitation. This result agrees with the early theoretical results of Schmitt-Rink *et al.*[26] and of Takagahara,[28] the early resonance Raman experiments of Scamarcio *et al.*,[17] and the more recent femtosecond pump−probe results of Salvador *et al.*[33] and Sagar *et al.*,[20] although not with some other theoretical and experimental reports.[11,29−31] Reduction in EPC with increased delocalization of the electronic wave functions is a familiar result in the spectroscopy of molecules and molecular aggregates. For example, across the series of linear polyenes, the smallest members (ethylene and butadiene) exhibit more extensive vibronic structure in their

absorption spectra than do the longer members (octatetraene and up),[46] and the optical spectra of J-aggregated dyes are characterized by a very strong electronic origin and negligible intensity in vibronic sidebands compared with the constituent monomers.[47] This analogy is expected to hold only for SC NCs in the size range corresponding to strong confinement, that is, radii considerably smaller than the Bohr radius of the bulk exciton, ~5.4 nm for CdSe.[48] Strongly confined NCs and bulk SCs differ qualitatively in the nature of both the electron–hole wave functions and the phonon modes, as evidenced, for example, in the much larger reorganization energy in bulk CdSe than in "large" strongly confined NCs. These calculations also find that the acoustic phonons have larger Huang–Rhys factors than the optical phonons by factors of roughly 2 to 8. This trend is in agreement with the recent femtosecond pump–probe studies by Sagar *et al.*,[20,21] while the opposite trend was obtained from the three-pulse photon echo experiments of McKimmie *et al.*[24]

The present calculations yield EPC strengths that are considerably larger than found in most experiments, although the total vibrational reorganization energy is still relatively small compared with reorganization energies accompanying electronic excitation in most molecules and, apparently, with that of bulk CdSe. For the optical modes, these calculations find S values in the 0.3–1.2 range (λ = 25–100 cm^{-1}). While some prior studies have found values this high,[15,24,32] other experimental values are lower[19,27] by as much as an order of magnitude.[20,21] The calculated acoustic mode EPCs of $S > 1$ ($\lambda > 50$ cm^{-1}) exceed experimental estimates by 1–2 orders of magnitude.[20–22,24] Not all of the experimental systems are directly comparable to those calculated here (*e.g.*, some were performed on larger particles or core–shell systems), and the emission spectra measured on single NCs are weighted toward those NCs whose emission was most stable to both "blinking" and spectral diffusion. While the range among EPCs obtained from different experiments, and even for different NCs in the same experiment, is quite large, it does appear that these calculations overestimate the absolute magnitude of the EPC. Possible reasons are discussed below.

The dependence of EPC on the nature of the electron and hole wave functions has rarely been addressed in the literature even though resonance Raman and femtosecond pump–probe experiments are often carried out at wavelengths that are resonant with higher-lying transitions. The present calculations find that the EPC for both acoustic and optical modes is considerably weaker for $1S_e$–$2S_{3/2}$ excitation than for $1S_e$–$1S_{3/2}$ excitation. This result agrees qualitatively with the conclusions of Sagar *et al.*, who found that the EPC for optical phonons, in particular, decreases rapidly with increasing excitation energy (*i.e.*, in the sequence $1S_e$–$1S_{3/2}$, $1S_e$–$2S_{3/2}$, $1P_e$–$1P_{3/2}$, $1S_e$–$2S_{1/2}$).

The calculated frequencies of the strongly coupled optical modes cluster slightly below 200 cm^{-1}, whereas experimental Raman spectra of CdSe NCs in this size range have their dominant peak in the 203–208 cm^{-1} range.[13,15,49] The Rabani force field applied to bulk CdSe gives a calculated frequency of about 212 cm^{-1} for the zone center Γ_1 (A_1) LO phonon,[41] in very good agreement with the experimental Raman frequency in the bulk.[50,51] Thus, these calculations predict that NCs undergo a greater reduction in the frequencies of the coupled optical modes relative to the bulk than is observed experimentally. The NCs studied here do have some calculated frequencies above 205 cm^{-1}, but all such modes have very weak EPCs. Examination of the mode character of the strongly and weakly coupled modes in the 185–215 cm^{-1} region shows that the modes with strong EPC, which mostly fall slightly below 200 cm^{-1}, are typically delocalized over the crystal and involve significant motions of a large number of atoms, while the weakly coupled modes calculated in the 205–210 cm^{-1} range tend to be comparatively localized. Experimental Raman spectra of CdSe NCs show a weak, broad shoulder in the 185–200 cm^{-1} region which is generally assigned as a surface optical phonon,[11–13,49,52] but the phonons in the 185–200 cm^{-1} region that are calculated to have strong EPC are not localized on the surface atoms. There is no clear explanation for the softening in the frequencies of the delocalized LO-type phonons in the NCs relative to the bulk, but it may be related to the absence of capping ligands or an external medium in the calculations.

This study seeks insight into the electron–phonon coupling in CdSe nanocrystals by using a well-tested empirical force field to calculate the structures and phonon frequencies and eigenvectors for crystals of varying sizes. This approach captures not only phonon confinement but also effects on the phonon modes of surface reconstruction and small deviations from spherical symmetry. While the model employed for the phonons is thus fairly realistic, the EPC calculations presented here have two principal limitations. First, the energy minimization and phonon calculations are performed in a vacuum; the surface atoms are uncapped, and there is no external medium. The presence of ligands on the surface atoms, or a shell of a different semiconductor, will affect the frequencies and mode characters of phonons that involve significant motion of surface atoms. The effects are expected to be larger for acoustic phonons, which involve overall "breathing" of the NC, than for the optical phonons. The other major limitation is the use of particle in a sphere envelope function with a very simple model for the Bloch functions for the electron and hole wave functions. Consistent with an empirical force field that involves only isotropic Coulombic and Lennard-Jones interactions, the electron and hole have been assigned

as point charges on the nuclei, distributed according to a spherically symmetric envelope function. While this is expected to capture the dominant effects of electron−hole pair creation on phonon motion, it may be a significant approximation. The choice of Bloch function delocalization was found to change the Huang−Rhys factor by an order of magnitude in prior calculations of the deformation potential coupling to a uniform elastic sphere model for the acoustic phonons.[27] Both of these limitations will be addressed in future work.

METHODS

Geometries and Phonon Modes. Calculations of the equilibrium geometries and phonon frequencies and eigenvectors of CdSe NCs were carried out using the General Utility Lattice Program (GULP).[53] This program was originally developed for calculating a variety of structural and thermodynamic properties, including phonon dispersion curves, for crystalline solids, but it also works efficiently for clusters of thousands of atoms. It generates both phonon frequencies and the eigenvectors needed to calculate electron−phonon coupling. First, the known bulk lattice parameters[41] were used to create a chunk of wurtzite CdSe, and all atoms beyond a certain radius from a selected origin were deleted. Atoms having only one nearest neighbor were then sequentially eliminated from the structure. Choosing different origins and radii produced some structures that were stoichiometric and others that had a significant excess (up to 11 atoms) of either cations or anions. GULP was then used to optimize the geometry of the cluster. The calculations employed the Rabani force field (Coulomb plus Lennard-Jones) for CdSe.[41] This force field has been employed successfully in a number of molecular dynamics calculations on both bulk[54−56] and nanoscale[57−59] CdSe. The phonon frequencies and eigenvectors were then generated at the optimized geometry, and the calculated reduced masses were used to normalize the Cartesian displacements to the true displacements corresponding to $q = 1$. Structures were displayed, and normal modes were visualized using visual molecular dynamics[60] with the NMWiz plugin (https://simtk.org/home/nmwiz).

Electron and Hole Wave Functions. The electron and hole wave functions corresponding to the two lowest-energy allowed absorption bands in CdSe NPs, denoted $1S_e-1S_{3/2}$ and $1S_e-2S_{3/2}$, were calculated as particle-in-a-sphere envelope functions multiplying the Bloch functions. As the lowest-energy conduction band state is fairly well-isolated, a simple particle-in-a-sphere model[61−64] was employed for the electron using an effective mass of 0.13.[15,64] The potential was taken to be zero inside the NP ($r \le r_0$) and 4 eV outside the particle ($r > r_0$), allowing for some penetration of the electron wave function outside the physical edge of the NP (the ionization potential of the electron is finite). To simplify numerical solution, the potential was assumed to be infinite beyond a larger radius r_{out}, whose exact value does not matter as long as it is large enough that the wave functions have decayed essentially to zero; for this problem, r_{out} was chosen to be 1 nm greater than r_0. It is then straightforward to diagonalize the radial Hamiltonian in a basis of the spherical Bessel functions that constitute the eigenstates of the problem $V = 0$ for $r \le r_{out}$, $V = \infty$ for $r > r_{out}$. The lowest-energy eigenstate was then taken to be the envelope function for the $1S_e$ conduction band state.

The wave functions for the valence-band (hole) states are complicated by valence-band mixing caused by spin−orbit coupling. The valence band is composed of p atomic orbitals on Se having angular momentum $\ell = 1$, which couple to the spin-1/2 hole to produce Bloch states of angular momentum $J = 3/2$ or $J = 1/2$. The eigenstates of the Hamiltonian must then be eigenstates of total angular momentum $F = J + L$, where L is the orbital angular momentum of the envelope function. The formulation and solution of this problem are discussed in many places.[65−69] For CdSe, the lowest-energy valence-band states originate from the $J = 3/2$ components (heavy hole and light hole) and are only weakly coupled to the $J = 1/2$ (split-off hole) component. States of total $F = 3/2$ and even parity originate from the combination of Bloch functions with $J = 3/2$ and envelope functions with $L = 0$ or $L = 2$. Thus, while the top of the valence band is generally referred to as $1S_{3/2}$, the corresponding envelope function is actually a combination of S-type and D-type functions. The $F = 3/2$ hole functions are four-fold degenerate ($M_F = 3/2, 1/2, -1/2$, and $-3/2$) and are given by[66]

$$\psi_M = 2\sum_{\ell=0,2} R_\ell(r)(-1)^{M-3/2}\sum_{m+\mu=M}\begin{pmatrix} 3/2 & \ell & 3/2 \\ \mu & m & -M \end{pmatrix} Y_\ell^m(\theta,\phi)u_\mu \tag{1}$$

where the u_μ is the Bloch function ($\mu = 3/2, 1/2, -1/2, -3/2$), the quantity in large parentheses is a Wigner 3j symbol, and Y_ℓ^m is a spherical harmonic that constitutes the angular part of the envelope function. The potential is taken to be infinite outside the crystal ($r > r_0$), a reasonable approximation for the holes which penetrate less into the classically forbidden region than the electrons because of their greater effective mass. The radial functions are then given by[66]

$$\begin{aligned} R_0(r) &= A\left[j_0(\varphi r/r_0) - \frac{j_0(\varphi)}{j_0(\varphi\sqrt{\beta})}j_0(\varphi\sqrt{\beta}r/r_0)\right] \\ R_2(r) &= A\left[j_2(\varphi r/r_0) + \frac{j_0(\varphi)}{j_0(\varphi\sqrt{\beta})}j_2(\varphi\sqrt{\beta}r/r_0)\right] \end{aligned} \tag{2}$$

where A is a normalization constant chosen such that $\int dr r^2[R_0^2(r) + R_2^2(r)] = 1$, j_ℓ is a spherical Bessel function, β is the ratio of light-hole to heavy-hole effective masses ($\beta = 0.28$ was used),[66] and ϕ is the first (for $1S_{3/2}$) or second (for $2S_{3/2}$) root of the equation

$$j_0(\varphi)j_2(\sqrt{\beta}\varphi) + j_2(\varphi)j_0(\sqrt{\beta}\varphi) = 0 \tag{3}$$

The EPC calculations require only the square of the wave function, which determines the charges on the atoms. Calculating $\Sigma_M|\psi_M|^2$ and integrating over the Bloch coordinates leaves the simple result that the square of the envelope function is spherically symmetric and has a radial part given by $R_0^2(r) + R_2^2(r)$.

Once the wave functions were calculated, the changes in charge distribution produced by electron−hole pair formation were calculated by assigning each Cd (Se) atom a charge equal to the square of the electron (hole) wave function at that point in space, normalizing the total charge to unity. The electron and hole were treated as point charges located at the centers of the atoms for consistency with the Rabani ground-state force field, which treats the Coulombic part of the potential as arising from point charges.

Electron−Phonon Coupling. The Huang−Rhys factor for each phonon mode i is given by $S_i = \Delta_i^2/2$, where Δ_i, the displacement between ground and excited electronic state minima along dimensionless coordinate i in the linear electron−phonon coupling limit, is given by $dE_{eg}/dq_i = \hbar\omega_i\Delta_i$, where E_{eg} is the energy difference between excited and ground states. The electrostatic energy due to Coulomb interactions is $E_C = \Sigma_i\Sigma_{j>i}(q_iq_j)/r_{ij}$, so E_{eg} is simply given by the difference between the Coulombic energy when the atoms have their ground-state charges and that when the atomic charges have been modified by electron−hole pair formation. The Lennard-Jones contribution to the energy was assumed to be identical in the ground and excited states. All calculations were carried out with the assumption of harmonic vibrations and linear electron−phonon coupling.

Resonance Raman Spectra. Resonance Raman spectra were calculated by assuming that the Raman intensity in mode *i* is proportional to $\Delta_i^2\omega_i^2$, the square of the slope of the excited-state potential energy surface along the ground-state dimensionless phonon coordinate, and assigning a Lorentzian line width of 4 cm^{-1} (fwhm) to each phonon transition. Resonance Raman intensities actually depend in a complex manner on the EPCs for all phonons as well as the homogeneous and inhomogeneous electronic line broadening, degree of detuning from resonance, and interference effects among multiple resonant transitions,[70] but $I \sim \Delta^2\omega^2$ is usually a good approximation for low-frequency vibrations and unstructured electronic spectra.[70−72] Overtone and combination band intensities also depend in a complex manner on a number of factors including the EPC strengths, the frequencies of the modes involved, and the electronic dephasing rates. Overtones and combination bands of low-frequency modes are typically strongly attenuated in Raman spectra relative to their intensities in a resolved absorption or emission spectrum. In view of the uncertainties involved, the Raman overtone and combination bands were not calculated. The approximation $I \sim \Delta^2\omega^2$ implicitly assumes that the temperature is low enough that most of the population starts in the vibrational ground state of all important vibrational modes, which effectively requires a temperature of 20−30 K or lower. Some deviations from the scaling of Raman intensity with displacement are expected at higher temperatures.

Acknowledgment. I thank M. E. Colvin, J. Gale, D. F. Kelley, and E. Rabani for helpful comments and advice at various stages in this work.

REFERENCES AND NOTES

1. Klimov, V. I. Spectral and Dynamical Properties of Multiexcitons in Semiconductor Nanocrystals. *Annu. Rev. Phys. Chem.* **2007**, *58*, 635–673.
2. Beard, M. C.; Midgett, A. G.; Hanna, M. C.; Luther, J. M.; Hughes, B. K.; Nozik, A. J. Comparing Multiple Exciton Generation in Quantum Dots To Impact Ionization in Bulk Semiconductors: Implications for Enhancement of Solar Energy Conversion. *Nano Lett.* **2010**, *10*, 3019–3027.
3. McGuire, J. A.; Joo, J.; Pietryga, J. M.; Schaller, R. D.; Klimov, V. I. New Aspects of Carrier Multiplication in Semiconductor Nanocrystals. *Acc. Chem. Res.* **2008**, *41*, 1810–1819.
4. Nozik, A. J. Multiple Exciton Generation in Semiconductor Quantum Dots. *Chem. Phys. Lett.* **2008**, *457*, 3–11.
5. Boulesbaa, A.; Issac, A.; Stockwell, D.; Huang, Z.; Huang, J.; Guo, J.; Lian, T. Ultrafast Charge Separation at CdS Quantum Dot/Rhodamine B Molecule Interface. *J. Am. Chem. Soc.* **2007**, *129*, 15132–15133.
6. Chuang, C.-H.; Lo, S. S.; Scholes, G. D.; Burda, C. Charge Separation and Recombination in CdTe/CdSe Core/Shell Nanocrystals as a Function of Shell Coverage: Probing the Onset of the Quasi Type-II Regime. *J. Phys. Chem. Lett.* **2010**, *1*, 2530–2535.
7. Dooley, C. J.; Dimitrov, S. D.; Feibig, T. Ultrafast Electron Transfer Dynamics in CdSe/CdTe Donor−Acceptor Nanorods. *J. Phys. Chem. C* **2008**, *112*, 12074–12076.
8. Kumar, S.; Jones, M.; Lo, S. S.; Scholes, G. D. Nanorod Heterostructures Showing Photoinduced Charge Separation. *Small* **2007**, *3*, 1633–1639.
9. Kelley, A. M. Electron−Phonon Coupling in CdSe Nanocrystals. *J. Phys. Chem. Lett.* **2010**, *1*, 1296–1300.
10. Shim, M.; Guyot-Sionnest, P. Intraband Hole Burning of Colloidal Quantum Dots. *Phys. Rev. B* **2001**, *64*, 245342.
11. Klein, M. C.; Hache, F.; Ricard, D.; Flytzanis, C. Size Dependence of Electron−Phonon Coupling in Semiconductor Nanospheres: The Case of CdSe. *Phys. Rev. B* **1990**, *42*, 11123–11132.
12. Baranov, A. V.; Rakovich, Y. P.; Donegan, J. F.; Perova, T. S.; Moore, R. A.; Talapin, D. V.; Rogach, A. L.; Masumoto, Y.; Nabiev, I. Effect of ZnS Shell Thickness on the Phonon Spectra in CdSe Quantum Dots. *Phys. Rev. B* **2003**, *68*, 165306.
13. Dzhagan, V. M.; Valakh, M. Y.; Raevskaya, A. E.; Stroyuk, A. L.; Kuchmiy, S. Y.; Zahn, D. R. T. Size Effects on Raman Spectra of Small CdSe Nanoparticles in Polymer Films. *Nanotechnology* **2008**, *19*, 305707.
14. Dzhagan, V. M.; Valakh, M. Y.; Raevska, O. E.; Stroyuk, O. L.; Kuchmiy, S. Y.; Zahn, D. R. T. The Influence of Shell Parameters on Phonons in Core-Shell Nanoparticles: A Resonant Raman Study. *Nanotechnology* **2009**, *20*, 365704.
15. Alivisatos, A. P.; Harris, T. D.; Carroll, P. J.; Steigerwald, M. L.; Brus, L. E. Electron-Vibration Coupling in Semiconductor Clusters Studied by Resonance Raman Spectroscopy. *J. Chem. Phys.* **1989**, *90*, 3463–3468.
16. Yu, P. Y.; Smith, J. E., Jr. Transformation from Raman Scattering to Photoluminescence at the C Exciton of CdSe. *Phys. Rev. Lett.* **1976**, *37*, 622–625.
17. Scamarcio, G.; Spagnolo, V.; Ventruti, G.; Lugara, M.; Righini, G. C. Size Dependence of Electron−LO−Phonon Coupling in Semiconductor Nanocrystals. *Phys. Rev. B* **1996**, *53*, R10489–R10492.
18. Lange, H.; Artemyev, M.; Woggon, U.; Niermann, T.; Thomsen, C. Experimental Investigation of Exciton−LO−Phonon Couplings in CdSe/ZnS Core/Shell Nanorods. *Phys. Rev. B* **2008**, *77*, 193303.
19. Mittleman, D. M.; Schoenlein, R. W.; Shiang, J. J.; Colvin, V. L.; Alivisatos, A. P.; Shank, C. V. Quantum Size Dependence of Femtosecond Electronic Dephasing and Vibrational Dynamics in CdSe Nanocrystals. *Phys. Rev. B* **1994**, *49*, 14435–14447.
20. Sagar, D. M.; Cooney, R. R.; Sewall, S. L.; Dias, E. A.; Barsan, M. M.; Butler, I. S.; Kambhampati, P. Size Dependent, State-Resolved Studies of Exciton-Phonon Couplings in Strongly Confined Semiconductor Quantum Dots. *Phys. Rev. B* **2008**, *77*, 235321.
21. Sagar, D. M.; Cooney, R. R.; Sewall, S. L.; Kambhampati, P. State-Resolved Exciton−Phonon Couplings in CdSe Semiconductor Quantum Dots. *J. Phys. Chem. C* **2008**, *112*, 9124–9127.
22. Fernée, M. J.; Littleton, B. N.; Cooper, S.; Rubinsztein-Dunlop, H.; Gomez, D. E.; Mulvaney, P. Acoustic Phonon Contributions to the Emission Spectrum of Single CdSe Nanocrystals. *J. Phys. Chem. C* **2008**, *112*, 1878–1884.
23. Chilla, G.; Kipp, T.; Menke, T.; Heitmann, D.; Nikolic, M.; Fromsdorf, A.; Kornowski, A.; Forster, S.; Weller, H. Direct Observation of Confined Acoustic Phonons in the Photoluminescence Spectra of a Single CdSe−CdS−ZnS Core−Shell−Shell Nanocrystal. *Phys. Rev. Lett.* **2008**, *100*, 057403.
24. McKimmie, L. J.; Lincoln, C. N.; Jasieniak, J.; Smith, T. A. Three-Pulse Photon Echo Peak Shift Measurements of Capped CdSe Quantum Dots. *J. Phys. Chem. C* **2010**, *114*, 82–88.
25. Huxter, V. M.; Lee, A.; Lo, S. S.; Scholes, G. D. CdSe Nanoparticle Elasticity and Surface Energy. *Nano Lett.* **2009**, *9*, 405–409.
26. Schmitt-Rink, S.; Miller, D. A. B.; Chemla, D. S. Theory of the Linear and Nonlinear Optical Properties of Semiconductor Microcrystallites. *Phys. Rev. B* **1987**, *35*, 8113–8125.
27. Salvador, M. R.; Graham, M. W.; Scholes, G. D. Exciton−Phonon Coupling and Disorder in the Excited States of CdSe Colloidal Quantum Dots. *J. Chem. Phys.* **2006**, *125*, 184709.
28. Takagahara, T. Electron−Phonon Interactions and Excitonic Dephasing in Semiconductor Nanocrystals. *Phys. Rev. Lett.* **1993**, *71*, 3577–3580.
29. Nomura, S.; Kobayashi, T. Exciton−LO−Phonon Couplings in Spherical Semiconductor Microcrystallites. *Phys. Rev. B* **1992**, *45*, 1305–1316.
30. Rodriguez-Suarez, R.; Menendez-Proupin, E.; Trallero-Giner, C.; Cardona, M. Multiphonon Resonant Raman Scattering in Nanocrystals. *Phys. Rev. B* **2000**, *62*, 11006–11016.
31. Melnikov, D. V.; Fowler, W. B. Electron−Phonon Interaction in a Spherical Quantum Dot with Finite Potential Barriers: The Fröhlich Hamiltonian. *Phys. Rev. B* **2001**, *64*, 245320.

32. Norris, D. J.; Efros, A. L.; Rosen, M.; Bawendi, M. G. Size Dependence of Exciton Fine Structure in CdSe Quantum Dots. *Phys. Rev. B* **1996**, *53*, 16347–16354.
33. Salvador, M. R.; Hines, M. A.; Scholes, G. D. Exciton–Bath Coupling and Inhomogeneous Broadening in the Optical Spectroscopy of Semiconductor Quantum Dots. *J. Chem. Phys.* **2003**, *118*, 9380–9387.
34. Fu, H.; Ozolins, V.; Zunger, A. Phonons in Gap Quantum Dots. *Phys. Rev. B* **1999**, *59*, 2881–2887.
35. Cheng, W.; Ren, S.-F.; Yu, P. Y. Theoretical Investigation of the Surface Vibrational Modes in Germanium Nanocrystals. *Phys. Rev. B* **2003**, *68*, 193309.
36. Ren, S.-F.; Lu, D.; Qin, G. Phonon Modes in InAs Quantum Dots. *Phys. Rev. B* **2001**, *63*, 195315.
37. Ren, S.-F.; Cheng, W.; Yu, P. Y. Microscopic Investigation of Phonon Modes in SiGe Alloy Nanocrystals. *Phys. Rev. B* **2004**, *69*, 235327.
38. Qin, G.; Ren, S.-F. Effects of Core Size and Shell Thickness on Phonon Modes in GaAs/AlAs Shell Quantum Dots. *J. Appl. Phys.* **2001**, *89*, 6037–6043.
39. Cheng, W.; Ren, S.-F. Calculations on the Size Effects of Raman Intensities of Silicon Quantum Dots. *Phys. Rev. B* **2002**, *65*, 205305.
40. Khoo, K. H.; Zayak, A. T.; Kwak, H.; Chelikowsky, J. R. First-Principles Study of Confinement Effects on the Raman Spectra of Si Nanocrystals. *Phys. Rev. Lett.* **2010**, *105*, 115504.
41. Rabani, E. An Interatomic Pair Potential for Cadmium Selenide. *J. Chem. Phys.* **2002**, *116*, 258–262.
42. Efros, A. L.; Rosen, M. The Electronic Structure of Semiconductor Nanocrystals. *Annu. Rev. Mater. Sci.* **2000**, *30*, 475–521.
43. Son, D. H.; Wittenberg, J. S.; Banin, U.; Alivisatos, A. P. Second Harmonic Generation and Confined Acoustic Phonons in Highly Excited Semiconductor Nanocrystals. *J. Phys. Chem. B* **2006**, *110*, 19884–19890.
44. Oron, D.; Aharoni, A.; de Mello Donega, C.; van Rijssel, J.; Meijerink, A.; Banin, U. Universal Role of Discrete Acoustic Phonons in the Low Temperature Optical Emission of Colloidal Quantum Dots. *Phys. Rev. Lett.* **2009**, *102*, 177402.
45. Markel, F.; Ferris, N. S.; Gould, I. R.; Myers, A. B. Mode-Specific Vibrational Reorganization Energies Accompanying Photoinduced Electron Transfer in the Hexamethylbenzene/Tetracyanoethylene Charge-Transfer Complex. *J. Am. Chem. Soc.* **1992**, *114*, 6208–6219.
46. Granville, M. F.; Kohler, B. E.; Snow, J. B. Franck-Condon Analysis of the $1^1A_g \rightarrow 1^1B_u$ Absorption in Linear Polyenes with Two through Six Double Bonds. *J. Chem. Phys.* **1981**, *75*, 3765–3769.
47. Nishimura, K.; Tokunaga, E.; Kobayashi, T. Sub-5-fs Two-Dimensional Spectroscopy of Pseudoisocyanine J-Aggregates. *Chem. Phys. Lett.* **2004**, *395*, 114–119.
48. Yoffe, A. D. Low-Dimensional Systems: Quantum Size Effects and Electronic Properties of Semiconductor Microcrystallites (Zero-Dimensional Systems) and Some Quasi-Two-Dimensional Systems. *Adv. Phys.* **2002**, *51*, 799–890.
49. Kusch, P.; Lange, H.; Artemyev, M.; Thomsen, C. Size-Dependence of the Anharmonicities in the Vibrational Potential of Colloidal CdSe Nanocrystals. *Solid State Commun.* **2011**, *151*, 67–70.
50. Hermann, C.; Yu, P. Y. Role of Elastic Exciton-Defect Scattering in Resonant Raman and Resonant Brillouin Scattering in CdSe. *Phys. Rev. B* **1980**, *21*, 3675–3688.
51. Arora, A. K.; Ramdas, A. K. Resonance Raman Scattering from Defects in CdSe. *Phys. Rev. B* **1987**, *35*, 4345–4350.
52. Comas, F.; Trallero-Giner, C.; Studart, N.; Marques, G. E. Interface Optical Phonons in Spheroidal Dots: Raman Selection Rules. *Phys. Rev. B* **2002**, *65*, 073303.
53. Gale, J. D.; Rohl, A. L. The General Utility Lattice Program (GULP). *Mol. Simul.* **2003**, *29*, 291–341.
54. Bealing, C.; Martonak, R.; Molteni, C. The Wurtzite to Rock Salt Transition in CdSe: A Comparison between Molecular Dynamics and Metadynamics Simulations. *Solid State Sci.* **2010**, *12*, 157–162.
55. Reed, E. J. Atomic Transformation Pathways from Terahertz Radiation Generated by Shock-Induced Phase Transformations. *Phys. Rev. B* **2010**, *81*, 144123.
56. Leoni, S.; Ramlau, R.; Meier, K.; Schmidt, M.; Schwarz, U. Nanodomain Fragmentation and Local Rearrangements in CdSe under Pressure. *Proc. Natl. Acad. Sci. U.S.A.* **2008**, *105*, 19612–19616.
57. Ye, X.; Sun, D. Y.; Gong, X. G. Pressure-Induced Structural Transformation of CdSe Nanocrystals Studied with Molecular Dynamics. *Phys. Rev. B* **2008**, *77*, 094108.
58. Grunwald, M.; Rabani, E.; Dellago, C. Mechanisms of the Wurtzite to Rocksalt Transformation in CdSe Nanocrystals. *Phys. Rev. Lett.* **2006**, *96*, 255701.
59. Grunwald, M.; Dellago, C. Transition State Analysis of Solid–Solid Transformations in Nanocrystals. *J. Chem. Phys.* **2009**, *131*, 164116.
60. Humphrey, W.; Dalke, A.; Schulten, K. VMD: Visual Molecular Dynamics. *J. Mol. Graphics* **1996**, *14*, 33–38.
61. Brus, L. E. A Simple Model for the Ionization Potential, Electron Affinity, and Aqueous Redox Potentials of Small Semiconductor Crystallites. *J. Chem. Phys.* **1983**, *79*, 5566–5571.
62. Dabbousi, B. O.; Rodriguez-Viejo, J.; Mikulec, F. V.; Heine, J. R.; Mattoussi, H.; Ober, R.; Jensen, K. F.; Bawendi, M. G. (CdSe)ZnS Core–Shell Quantum Dots: Synthesis and Characterization of a Size Series of Highly Luminescent Nanocrystallites. *J. Phys. Chem. B* **1997**, *101*, 9463–9475.
63. Haus, J. W.; Zhou, H. S.; Honma, I.; Komiyama, H. Quantum Confinement in Semiconductor Heterostructure Nanometer-Size Particles. *Phys. Rev. B* **1993**, *47*, 1359–1365.
64. Zhu, H.; Song, N.; Lian, T. Controlling Charge Separation and Recombination Rates in CdSe/ZnS Type I Core–Shell Quantum Dots by Shell Thicknesses. *J. Am. Chem. Soc.* **2010**, *132*, 15038–15045.
65. Efros, A. L. Luminescence Polarization of CdSe Microcrystals. *Phys. Rev. B* **1992**, *46*, 7448–7458.
66. Efros, A. L.; Rosen, M.; Kuno, M.; Nirmal, M.; Norris, D. J.; Bawendi, M. Band-Edge Exciton in Quantum Dots of Semiconductors with a Degenerate Valence Band: Dark and Bright Exciton States. *Phys. Rev. B* **1996**, *54*, 4843–4856.
67. Ekimov, A. I.; Hache, F.; Schanne-Klein, M. C.; Ricard, D.; Flytzanis, C.; Kudryavtsev, I. A.; Yazeva, T. V.; Rodina, A. V. Absorption and Intensity-Dependent Photoluminescence Measurements on CdSe Quantum Dots: Assignment of the First Electronic Transition. *J. Opt. Soc. Am. B* **1993**, *10*, 100–107.
68. Richard, T.; Lefebvre, P.; Mathieu, H.; Allegre, J. Effects of Finite Spin–Orbit Splitting on Optical Properties of Spherical Semiconductor Quantum Dots. *Phys. Rev. B* **1996**, *53*, 7287–7298.
69. Sercel, P. C.; Vahala, K. J. Analytical Formalism for Determining Quantum-Wire and Quantum-Dot Band Structure in the Multiband Envelope-Function Approximation. *Phys. Rev. B* **1990**, *42*, 3690–3710.
70. Myers, A. B. Excited Electronic State Properties from Ground-State Resonance Raman Intensities. In *Laser Techniques in Chemistry*; Myers, A. B., Rizzo, T. R., Eds.; Wiley: New York, 1995; pp 325–384.
71. Myers, A. B.; Mathies, R. A. Resonance Raman Intensities: A Probe of Excited-State Structure and Dynamics. In *Biological Applications of Raman Spectroscopy*; Spiro, T. G., Ed.; Wiley: New York, 1987; Vol. 2, pp 1–58.
72. Harris, R. A.; Mathies, R.; Myers, A. A Simple Sum Rule in Raman Theory. *Chem. Phys. Lett.* **1983**, *94*, 327.